

PHYSICS CONTRIBUTION

IMPROVED TREATMENT PLANNING FOR COMS EYE PLAQUES

MELVIN A. ASTRAHAN, PH.D.

Department of Radiation Oncology, University of Southern California Norris Cancer Hospital, Los Angeles, CA

Purpose: A recent reanalysis of the Collaborative Ocular Melanoma Study (COMS) medium tumor trial concluded that incorporating factors to account for anisotropy, line source approximation, the gold plaque, and attenuation in the Silastic seed carrier into the dose calculations resulted in a significant and consistent reduction of calculated doses to structures of interest within the eye. The authors concluded that future eye plaque dosimetry should be “performed using the most up-to-date parameters available.” The reason these factors are important is attributable to the low energy ^{125}I radiation (approximately 28 keV) that is primarily absorbed by the photoelectric process. Photoelectric absorption is quite dependent on the atomic composition of the absorbing material. Being 40% silicon by weight, the effective atomic number of Silastic is significantly greater than that of water. Although the AAPM TG43 brachytherapy formalism inherently addresses the issues of source anisotropy and geometry, its parameter that accounts for scatter and attenuation, the radial dose function $g(r)$, assumes that the source is immersed in infinite homogeneous water. In this work, factors are proposed for ^{125}I that correct for attenuation in the Silastic carrier and scatter deficits resulting from the gold plaque and nearby air. The implications of using ^{103}Pd seeds in COMS plaques are also discussed.

Methods and Materials: An existing TG43-based ophthalmic plaque planning system was modified to incorporate additional scatter and attenuation correction factors that better account for the path length of primary radiation in the Silastic seed carrier and the distance between the dose calculation point and the eye-air interface.

Results: Compared with homogeneous water, the dose-modifying effects of the Silastic and gold are greatest near the plaque surface and immediately adjacent to the plaque, while being least near the center of the eye. The calculated dose distribution surrounding a single ^{125}I seed centered in a COMS 20 mm plaque was found to be consistent with previously published examples that used thermoluminescent dosimetry measurements and Monte Carlo methods. For fully loaded 12 and 20 mm plaques, calculated dose to critical ocular structures ranged from 16%–50% less than would have been reported using the standard COMS dose calculation protocol.

Conclusions: Treatment planning for COMS eye plaques that accurately accounts for the presence of the gold, Silastic and extraocular air is both possible and practical. © 2005 Elsevier Inc.

Eye plaque, Seed carrier, Silastic, Dosimetry, ^{125}I , ^{103}Pd .

INTRODUCTION

The Collaborative Ocular Melanoma Study (COMS) is a multicenter investigation begun in the mid 1980s whose purpose was to evaluate the role of radiation therapy in the treatment of choroidal melanoma. The medium tumor trial of the COMS was designed to compare patient survival after randomization between enucleation and episcleral plaque therapy. A recent report indicates that survival rates for the two treatments are about the same (1).

The COMS study mandated the use of ^{125}I , provided a standardized set of plaques, and enforced a strict set of dosimetric assumptions. The COMS plaque designs have been discussed in the literature (2–5). Briefly, they consist of a 0.5-mm thick bowl-like gold alloy backing (77% gold, 14% silver, 8% copper, and 1% palladium) with a cylindrical collimating lip and a Silastic seed carrier into which the ^{125}I seeds are loaded. The carrier offsets the seeds by 1 mm

from the concave (front) surface of the plaque. The COMS dosimetric assumptions (D_{COMS}) require that the ^{125}I seeds be treated as point sources, that source anisotropy and the effects of the gold backing on scatter and attenuation be ignored, that the Silastic insert of the plaque be assumed to be water equivalent, and that shielding effects of the collimating lip be ignored. A recent reanalysis of the medium tumor trial data by Krintz *et al.* (6) concluded that incorporating factors to account for anisotropy, line source approximation, the gold plaque, and attenuation in the Silastic seed carrier into the dose calculations resulted in a significant and consistent reduction of calculated doses to structures of interest within the eye.

The reason that these factors are important is attributable to the soft (low) energy of the radiation sources used in these plaques. ^{125}I decays by electron capture to an excited state of ^{125}Te . Characteristic X-rays in the range 27–35 keV

are emitted along with 35.5 keV γ photons resulting from the decay of ^{125}I to its ground state. Some models of ^{125}I seeds that contain silver markers also emit fluorescent (characteristic) X-rays at 22 and 25 keV. Titanium encapsulation absorbs liberated electrons and very low energy X-rays. In 1999, however, the National Institute of Standards and Technology (NIST) revised its calibration procedures for ^{125}I to account for the presence of 4.5 keV titanium characteristic X-rays that do not contribute to dose in water at distances beyond 1 mm. For the purposes of this work, ^{125}I will be considered to emit photons with an average energy of 28 keV. Another isotope that has recently been proposed for eye plaque therapy (7, 8) is ^{103}Pd , which also decays by electron capture with the emission of characteristic X-rays in the range 20–23 keV (average energy approximately 21 keV).

For photons of these energies, the photoelectric effect is the dominant process by which energy is absorbed in common materials. Because the photoelectric mass attenuation coefficient is roughly proportional to the cube of the atomic number (Z) of the absorbing material, inhomogeneities in the immediate vicinity of an ^{125}I or ^{103}Pd seed can significantly affect the absorbed dose distribution. For instance, anisotropy resulting from self-absorption is severe for these seeds.

The AAPM TG43 brachytherapy formalism (9), which now forms the basis for most commercial brachytherapy planning systems, is also recommended by the COMS Manual of Procedures (10) for COMS dosimetry. Although TG43 inherently addresses the issues of source anisotropy and geometry (i.e., linear vs. point source) mentioned by Krintz *et al.* (6), the TG43 parameter that accounts for scatter and attenuation, the radial dose function $g(r)$, assumes that the source is immersed in infinite homogeneous water. Calculating dose to water is an acceptable practice because the effective atomic numbers of ocular tissues, and therefore their scattering and attenuation properties, are fairly close to those of water. The effective atomic number (Z_{eff}) is the atomic number of a hypothetical single element that would attenuate photons at the same rate as a composite material.

The COMS Silastic carrier has been reported (4) to be made of Dow Corning medical grade elastomer, MDX4-4210. Table 1 compares the fractional elemental composition by weight, density, and effective atomic number of water, eye lens, blood, and Silastic. The composition of Silastic was taken from Table 1 in Chiu-Taso *et al.* (4). The elemental composition of the other materials was obtained from an online NIST database (11). The Z_{eff} was calculated using the method of Mayneord (12) as described in Khan (13) as:

$$Z_{\text{eff}} = (a_1 Z_1^{2.94} + a_2 Z_2^{2.94} + a_3 Z_3^{2.94} + \dots + a_n Z_n^{2.94})^{1/2.94} \quad (1)$$

where $a_1, a_2, a_3, \dots, a_n$ are the fractional contributions of each element to the total number of electrons in the mixture.

Table 1. Fraction by weight elemental composition, density, and calculated Z_{eff} of some materials discussed in this report

Element	Z	Water	Eye Lens	Blood	Silastic
H	1	0.1119	0.096	0.102	0.063
C	6		0.195	0.110	0.249
N	7		0.057	0.033	
O	8	0.8881	0.646	0.745	0.289
Na	11		0.001	0.001	
Si	14				0.399
P	15		0.001	0.001	
S	16		0.003	0.002	
Cl	17		0.001	0.003	
K	19			0.002	
Fe	26			0.001	
Pt	78				0.00005
ρ		1.0	1.07	1.06	1.12
Z_{eff}		7.4	7.2	7.5	10.7

Mass attenuation coefficients (μ/ρ) expressed in cm^2/g (11) for monoenergetic photons corresponding to the average energies (E_{avg}) of ^{125}I (approximately 28 keV) and ^{103}Pd (approximately 21 keV) are plotted in Fig. 1 for materials with effective atomic numbers between 5 and 15. Summarized in Table 2 are some useful constants for Lucite (acrylic), water, Silastic, and gold that are readily derived from the mass attenuation coefficients: the linear attenuation coefficient (μ), the half value thickness ($\text{HVL} = 0.693/\mu$),

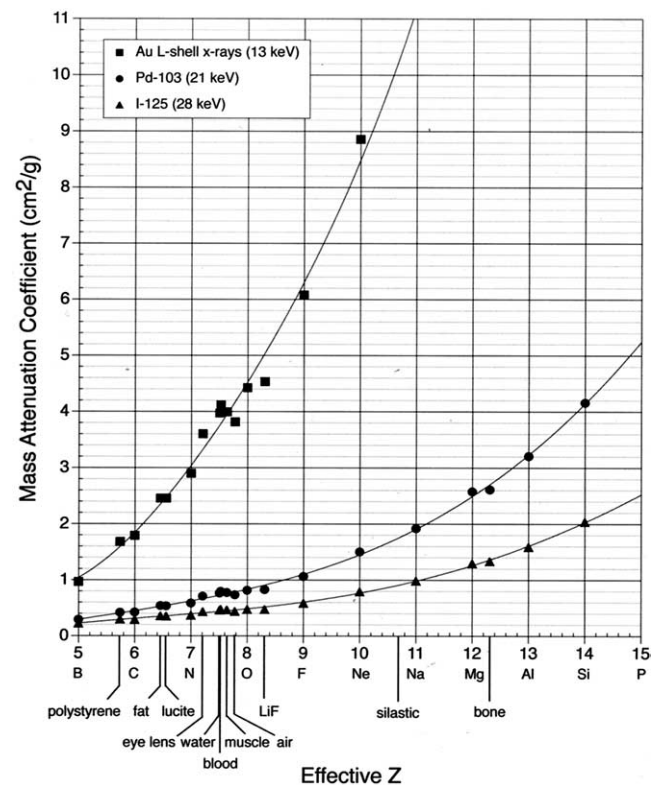


Fig. 1. Total mass attenuation coefficient (μ/ρ) expressed in cm^2/g for monoenergetic photons corresponding to the average energies (E_{avg}) of ^{125}I , ^{103}Pd , and gold L shell fluorescent (characteristic) X-rays.

Table 2. Some physical constants for materials and energies of interest in this work. For gold, the mass attenuation coefficients at 21 and 28 keV were calculated from a power fit to the tabulated data (11) over the range 15 to 80 keV ($\mu/\rho = e^{12.10799 * E_{avg} - 2.586464}$). For 13 keV (Au L X-rays) and other materials, linear interpolation was used

Radiation	E_{avg} keV	Lucite ($Z_{eff} = 6.56, \rho = 1.18$)				Water ($Z_{eff} = 7.4, \rho = 1$)				Silastic ($Z_{eff} \approx 10.7, \rho \approx 1.12$)				Gold ($Z = 79, \rho = 19.31$)			
		μ/ρ cm ² /g	μ cm ⁻¹	HVL cm	MFP cm	μ/ρ cm ² /g	μ cm ⁻¹	HVL cm	MFP cm	μ/ρ cm ² /g	μ cm ⁻¹	HVL cm	MFP cm	μ/ρ cm ² /g	μ cm ⁻¹	HVL cm	MFP cm
¹²⁵ I	28	0.35	0.42	1.67	2.40	0.46	1.52	2.19	0.90	1.01	0.69	0.99	32.8	633	1.1E-3	1.6E-3	
¹⁰³ Pd	21	0.54	0.64	1.01	1.58	0.77	0.92	1.33	1.75	1.96	0.35	0.51	69.0	1332	5.2E-4	7.5E-4	
Au L X-rays	13	2.46	2.90	0.24	0.34	3.97	0.13	0.19	10.2	11.4	0.06	0.09	150	2897	2.4E-4	3.4E-4	

and the mean free path (MFP = μ^{-1}). If a large number of photons of identical energy are incident upon an absorber of infinite thickness, then the MFP is the average, or mean distance traveled by any photon before a first collision. In 1 MFP of absorber the uncollided photon flux will be reduced to 1/e (0.37) of its original value.

Being 40% silicon (Z = 14) by weight, the effective atomic number of Silastic is close to 11, significantly higher than that of water, blood, or eye lens. For ¹²⁵I photons, the linear attenuation coefficient (μ) of Silastic (approximately 1.01 cm⁻¹) is about 2.2 times greater than that of water (0.46 cm⁻¹), and for ¹⁰³Pd, about 2.6 greater than that of water. The dose-modifying effects of the Silastic for ¹²⁵I radiation have been modeled using Monte Carlo methods by Chiu-Tsao *et al.* (4) and measured using thermoluminescent dosimeters (TLD) by Zerda *et al.* (5). They concluded that the effect of the Silastic insert and gold plaque was a dose reduction (compared with water) of about 10% at 1 cm on axis and about 15% at 2 cm and at off-axis points. The dose reduction in the Silastic insert will be even greater for ¹⁰³Pd radiation.

In addition to the Silastic carrier, the gold (Z = 79) backing, lip, and neighboring seeds are examples of nearby objects whose elemental compositions are also very different from water (Z_{eff} approximately 7.4). Dose enhancement (compared with water) close to a plaque from gold L-shell fluorescent X-rays (L1 = 14.4 keV, L2 = 13.7 keV, and L3 = 11.9 keV), and the modifying effects of the gold backing on scattered ¹²⁵I radiation have been discussed extensively in the literature (14–19).

Attempts to account for collimation of primary radiation by the gold backing and lip of the plaque in treatment planning have been reported by Astrahan *et al.* (3), Chiu-Tsao *et al.* (4), and Zerda *et al.* (5). With the HVL of ¹²⁵I radiation in pure gold being about 0.01 mm, transmission through the 0.5 mm thick gold alloy plaque can be considered to be zero. There will occur, however, a penumbral region, as illustrated in Fig. 2, whose properties depend on the proximity and orientation of the seeds with respect to the collimating lip. For the low energy of ¹²⁵I radiation, charged particle equilibrium can be assumed in the penumbral region (unlike a megavoltage beam) and transmission penumbra at the terminus of the lip can be ignored for practical purposes. The geometrical relationship between a seed and the lip, however, can create significant geometric penumbra because the active length of a seed (approximately 3 mm) is comparable to the height of the lip (approximately 3 mm). To address geometric penumbra, Astrahan *et al.* (3) implemented a general purpose line-of-sight approach that calculates the fraction of a linear source that is visible above the lip horizon (see Fig. 2). Zerda *et al.* (5) used TLD in a solid water phantom to measure planar dose distributions for a single ¹²⁵I seed centered in a 20 mm plaque and then used a modified Fermi-Dirac function to model the off-axis penumbral characteristics in both the transverse and longitudinal planes of the seed. This approach is derived from the two-dimensional (2D) methods used to characterize tele-

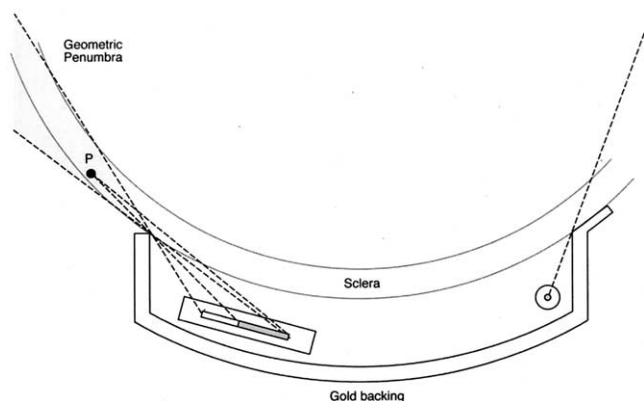


Fig. 2. Geometric penumbra for a linear source varies according to the proximity and orientation of the seed with respect to the collimating lip of the gold plaque. The dose rate at point P can be estimated from that portion of the active length of a source that is visible above the lip horizon when looking from P toward the source. The visible portion of the active length is shaded in this figure. To protect critical structures adjacent to the plaque, a source should run parallel to, and as close as possible to, the collimating lip as depicted on the right side of the figure.

therapy beams. In that situation, there is a single source, a single collimation system, and a fixed geometric relationship between the source and collimator. While potentially accurate, their method is inconvenient for eye plaques because it requires additional measurements or correction factors to account for all of the possible seed locations, orientations, and shapes of plaques. There now exist many different models of ^{125}I seeds. Plaques come in many shapes and sizes, some with notches in the lip for a snug fit to the optic nerve. Alternatively, Fluhs *et al.* (20) have described a measuring system that mechanically scans the entire three-dimensional (3D) dose rate distribution surrounding an eye plaque using a small volume (1 mm^3) plastic scintillator detector. This 3D dataset is used directly in their treatment planning process.

In this report, the dominant dosimetric reductions and enhancements relative to water produced by the Silastic carrier, the gold plaque, and air in front of the eye will be explored. Correction factors will be proposed that may be used with the TG43 formalism. The more complex dosimetric effects arising from interactions between adjacent seeds and extraocular inhomogeneities such as the lead-lined eye patches worn by patients and orbital bone will be ignored. These inhomogeneities presumably cause insignificant dosimetric changes and are better suited to Monte Carlo methods.

Background

Chiu-Tsao *et al.* (4) used Monte Carlo methods to model a single ^{125}I seed (model 6711) centered in the Silastic carrier of a 20 mm COMS plaque immersed in homogeneous water. In a follow-up study, Zerda *et al.* (5) used TLD to measure planar dose distributions in a solid water head phantom with an eye-air interface for the same source

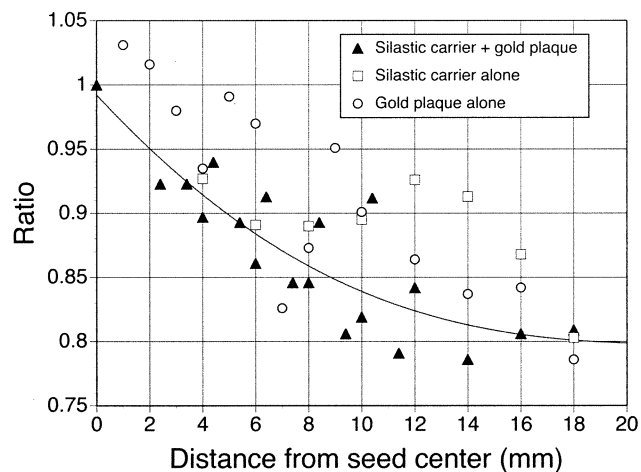


Fig. 3. The ratio of dose as calculated by the Monte Carlo method for a single ^{125}I seed centered in the carrier of a 20 mm COMS (Collaborative Ocular Melanoma Study) plaque to the dose in homogeneous water, as a function of transverse distance from the source axis. These data were manually redrawn from Figs. 5 and 6 in Chiu-Tsao *et al.* (4).

geometry. They concluded that the central axis dose reduction compared with homogeneous water is about 10% at 1 cm, and 15% at 2 cm and at off-axis points. Chiu-Tsao *et al.* (4) also noted that removal of the gold backing from the plaque “did not make a measureable difference in the dose reduction results” at 1 cm. This surprising observation warrants a closer look at their data and the underlying physics. The data points, less error bars, from Figs. 5 and 6 in Chiu-Tsao *et al.* (4) are redrawn here on an expanded vertical scale in Fig. 3. An extra point has been added in Fig. 3 at 0 mm for curve fitting purposes. These data were obtained by Monte Carlo methods and represent the ratio of dose for the Silastic insert alone, the gold backing alone, and the Silastic-plus-gold combination immersed in infinite water (i.e., no eye-air interface) to the dose in homogeneous water, plotted as a function of distance along the plaque central axis, which is also the seed transverse axis.

The linear attenuation coefficient μ represents the probability per photon per unit path length that a photon interaction will occur. For the energies of interest in this work, μ can be simplified to the sum of two components: $\mu = (\tau + \sigma)$, where τ is the photoelectric linear absorption coefficient and σ is the total Compton linear attenuation coefficient. For simplicity, the photoelectric process will be considered as purely absorptive and the Compton process considered as partly absorptive and partly scattering. Plotted in Figs. 4a, b, and c are the relative importance of the total Compton and photoelectric processes in water, Silastic and gold as a function of photon energy. The two processes have roughly equal probabilities of occurrence at 26 keV in water, 40 keV in Silastic, and 480 keV in gold. In the range 10–30 keV, photoelectric absorption accounts for virtually all of the interactions in gold and the majority of interactions with Silastic. Only in water (or water equivalent mixtures) does Compton scattering play a significant role.

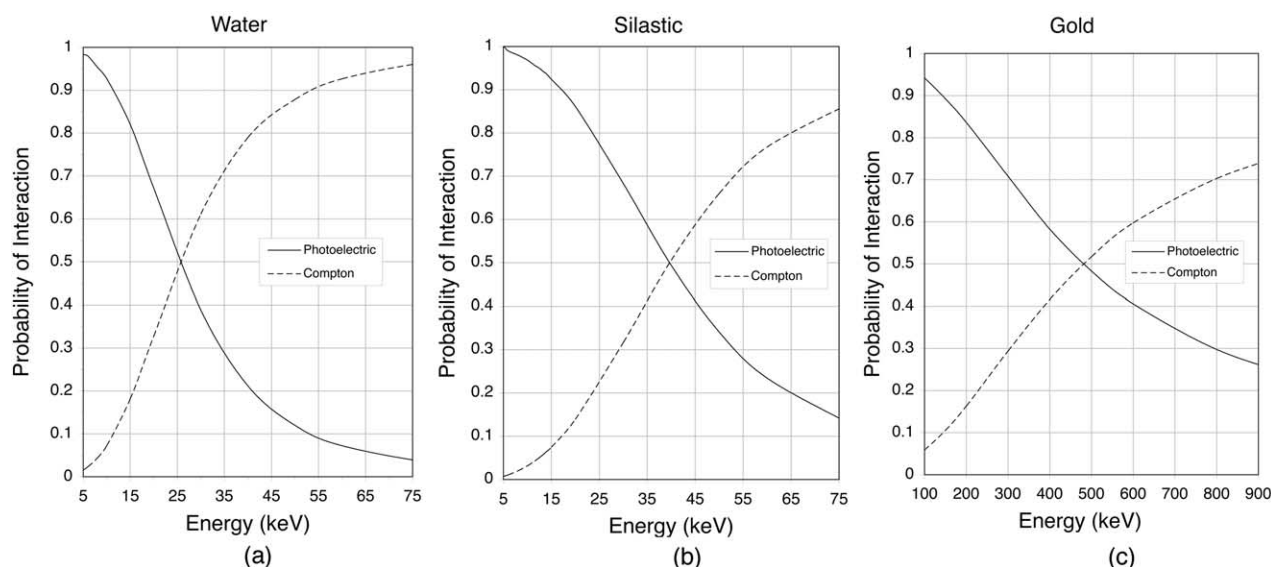


Fig. 4. Relative probability of photoelectric and Compton interactions as a function of photon energy for (a) water, (b) Silastic, and (c) gold. For ^{125}I radiation (E_{avg} approximately 28 keV), the chances of photoelectric and Compton interactions are nearly equal in water. Photoelectric absorption dominates in Silastic and is responsible for virtually all interactions in gold.

For incident-photons of low energy ($h\nu_0$), Compton scattering transfers only a small fraction of the total energy to the recoil electron and the angular distribution of the differential Compton scattered photons per unit solid angle is approximately symmetric around $\varphi = 90$ degrees as illustrated in Fig. 5. The energy of a Compton scattered photon ($h\nu'$) can be calculated as: $h\nu' = h\nu_0 (1 / [1 + \alpha(1 - \cos \varphi)])$, where $\alpha = (h\nu_0 / m_0c^2)$ and φ is the angle of photon scatter. The quantity $m_0c^2 = 511$ keV is the rest energy of an electron. For photons in the energy range of ^{125}I and ^{103}Pd plaque therapy, Compton scattering at φ approximately 90 degrees results in an energy loss per interaction of 2%–5% of the incident energy (see Table 3). The small energy loss per Compton interaction means that, even in water where the number of Compton interactions is significant, the dose delivered by Compton interactions will be small compared with the dose delivered by photoelectric absorption. Furthermore, the probability of subsequent interactions for the scattered photon will be nearly the same as for the incident photon. Dale (21) used Monte Carlo methods to explore this in more detail.

Now, consider an ^{125}I source surrounded by infinite water. About half of the emitted primary photons will undergo photoelectric absorption as their first interaction with the surrounding water. Most of these interactions will occur within one MFP (approximately 2 cm, roughly the diameter of an eye!) of the source. The other half will experience a Compton scattering interaction with an average directional change of about 90 degrees. Because the energy loss per Compton interaction is small, about half of the once-scattered photons will undergo photoelectric absorption as their next interaction, and half will experience a second Compton interaction. Of the twice-scattered photons, about half will undergo photoelectric absorption as their next interaction,

and half will experience a third Compton interaction. Less than 7% of the originally emitted photons will survive four interactions with the surrounding water, and those photons that do survive the first four interactions will have delivered very little absorbed dose. Since these low energy photons cannot scatter very many times before they are photoelectrically absorbed, the dosimetric effects of inhomogeneities (e.g., the gold backing and extraocular air) that produce changes in backscatter are likely to be range limited phenomena. Inhomogeneities that directly affect photoelectric attenuation (e.g., primary attenuation in the Silastic carrier) should have a more universal influence.

Figure 6 is a highly simplified interaction model of a low energy isotropic point source located at the center of an infinite sphere of water. Symmetry allows the sphere, and therefore photon interactions within the sphere, to be collapsed onto a 2D planar surface for the purposes of this discourse. The sphere, illustrated as a circle, is divided into front and rear hemispheres that are divided by a bisecting plane of symmetry depicted by the dashed horizontal line. The average direction of emitted photons with respect to this plane of symmetry are represented by the arrows. Half of the primary photons are emitted into the front hemisphere, the other half into the rear hemisphere. Now, consider only the primary photons emitted into the rear hemisphere. For ^{125}I , as mentioned above, about half of these photons will undergo photoelectric absorption within a couple of cm of the source as their first interaction with the surrounding water. The other half will experience a Compton scattering interaction. The average Compton scattering angle is assumed to be close to 90 degrees in this model. Since the energy of these once-scattered photons will be almost the same as the primary photons, about half will undergo photoelectric absorption as their next interaction

within a couple of cm of the first interaction. The once-scattered photons that are not photoelectrically absorbed will experience a second Compton interaction with, once again, an average scattering angle of roughly 90 degrees. Of these twice-scattered photons, half will be directed back toward the front hemisphere, the other half will proceed deeper into the rear hemisphere. This admittedly simple model predicts that roughly 12.5% of the photons originally emitted into the rear hemisphere will scatter back toward the front hemisphere. Of these once backscattered photons, a similar fraction will probably double back once again and return to the rear hemisphere. As was pointed out above, it is unlikely that many photons will survive more than four interactions before they are absorbed. The net result predicted by our model is that about 11% of the photons originally emitted into the rear hemisphere may actually wind up being absorbed in the front hemisphere. Applying the same conceptual model to ^{103}Pd , for which the probability of photoelectric absorption in water is about 70%, scatter from the rear into the front hemisphere should be closer to 5%. Due to symmetry, the same fraction of photons originally emitted into the front hemisphere will scatter back to the rear hemisphere, and an equilibrium condition will exist between the two hemispheres.

When the source is entirely surrounded by infinite water we have what is commonly referred to as full scatter geometry. Imagine now that the rear hemisphere consists entirely of air instead of water. Under these conditions very few photons emitted into the rear hemisphere will scatter back into the front hemisphere. Our model predicts that about 11% of the absorbed dose in each hemisphere can be attributed to photons that were originally emitted into the opposite hemisphere. If there is no backscatter from the rear hemisphere, dose in the front hemisphere should be about 11% less than it would be for the comparable full scatter geometry. Weaver (14) reported that with air backing an array of four ^{125}I seeds the measured dose at 15 mm depth in a polystyrene phantom was reduced by 9% compared with the full scatter geometry. Luxton *et al.* (15) measured a 10%–14% dose reduction in an acrylic phantom compared with full scatter over the range 10–18 mm in front of a single ^{125}I seed. Cygler *et al.* (17) calculated a dose reduction of about 10% at 10 mm in water for air backing compared with water backing for a single ^{125}I source.

Figure 7 conceptualizes interactions in the vicinity of the same low energy isotropic point source of Fig. 6, with the exception that it is now surrounded by the gold backing of an eye plaque on one side and water and air on the other side. When a gold backing is present, our model assumes that all photons emitted into the rear hemisphere immediately encounter the high Z gold where they are all photoelectrically absorbed. If all photons emitted into the rear hemisphere are absorbed in the gold, then none of those photons will scatter back into the front hemisphere, a situation nearly identical to that described above in which the rear hemisphere consisted of air. Dose in the front hemisphere should therefore also be about 11% less than it would

be for the homogeneous full scatter geometry. The dosimetric effects of various types of backings including gold and silver have been reported by several investigators (14–19). Weaver (14) reported that a sheet of gold backing reduced dose by 9% compared with full scatter in polystyrene at 15 mm in front of an array of four ^{125}I seeds. Luxton *et al.* (15) measured a 7%–10% reduction in acrylic compared with full scatter over the range 10–18 mm in front of a single ^{125}I seed that was backed by a nominally 15 mm diameter gold plaque. Cygler *et al.* (17) measured diode response reductions of about 7%–9% over the range 10–20 mm in water for a single ^{125}I seed with gold backing compared with water backing. Although the data in Fig. 3 are noisy, over the range 6–16 mm the average ratio of dose for the gold plaque alone to dose in homogeneous water is about 0.87 (13% reduction).

Interestingly, metallic backings do not simply eliminate backscatter from originating behind the plaque. As is also depicted in Fig. 7, with a gold backing, L-shell fluorescent X-rays resulting from the photoelectric absorption of ^{125}I photons in the gold are emitted back into the front hemisphere. These X-rays have a mean energy of about 13 keV, which means they have a MFP in water of around 2 mm. One would therefore expect most of these fluorescent X-rays to be absorbed within about 6 mm of the plaque. Cygler *et al.* (17) have pointed out that most of these fluorescent X-rays will never escape the 0.5 mm thick gold shield because their MFP in gold (3E-4 cm) is less than half that of the 28 keV photons (1.6E-3 cm) responsible for their creation. If the number of gold fluorescent X-rays entering the region just in front of the plaque exceeds the number of photons lost from that same region by lack of backscatter, a dosimetric enhancement compared with the full scatter condition will occur within that region. In Fig. 3, looking at the data for gold alone, a small dose enhancement is seen in the first few mm from the source axis. Luxton *et al.* (15) measured a 2% enhancement compared with full scatter at 2 mm in front of a single ^{125}I seed backed by a gold plaque. Cygler *et al.* (17) measured diode response enhancements of up to 7% at 2 mm in water for a single ^{125}I seed with gold backing compared with water backing. Meli and Motakabir (19) measured a diode response enhancement of only about 1% at 2 mm depth in water for gold backing compared with water backing.

Figure 7 also reminds us that photons that enter the air located in the front hemisphere can be considered lost as a source of scatter. The result will be a reduction of dose in the water near the water-air interface compared with the full scatter geometry.

In Fig. 8 our source is now embedded in the Silastic carrier of a COMS eye plaque. Silastic has a higher effective atomic number ($Z = 10.7$ vs. 7.4) and slightly higher density (ρ approximately 1.1 vs. 1.0) than water resulting in greater attenuation in the Silastic than would occur in an equal path length of water. For 28 keV photons the probability of photoelectric interaction in Silastic is about 75% (compared with approximately 50% in water) so a greater

Table 3. Energy of a Compton scattered photon

Radiation	Incident ($h\nu_0$) keV	α	Scattered ($h\nu'$, $\varphi = 90^\circ$) keV
^{125}I	28	0.055	26.5
^{103}Pd	21	0.041	20.2
Au L X-rays	13	0.025	12.7

proportion of that attenuation will be photoelectric. Primary photons emitted into the front hemisphere must pass through a minimum of 1 mm of Silastic. It will be shown later in this report that for a fully loaded COMS plaque, the mean linear path length through Silastic (MLPS) toward the apex of a medium height tumor is approximately 1.1 mm, and about 2.2 mm at the tumor base. Taking a median value in tumor for the MLPS of 1.7 mm (see Fig. 13), attenuation in the Silastic carrier would be about $e^{-\mu x} = e^{-1.01 * 0.17} = 0.842$ vs. $e^{-0.46 * 0.17} = 0.925$ of water. For ^{125}I , the ratio of attenuation in Silastic to attenuation in water should be about $0.842 / 0.925 = 0.91$. For ^{103}Pd , attenuation in the Silastic carrier will be greater than for ^{125}I . The ratio to water will be about $e^{-1.96 * 0.17} / e^{-0.75 * 0.17} = 0.717 / 0.880 = 0.81$.

Primary photons emitted into the rear hemisphere must also pass through Silastic. If we assume an average rearward path in Silastic of 1 mm the ratio of attenuation in Silastic to attenuation in water will be about $e^{-1.01 * 0.1} / e^{-0.46 * 0.1} = 0.904 / 0.955 = 0.946$ for ^{125}I , and about 0.886 ($e^{-1.96 * 0.1} / e^{-0.75 * 0.1}$) for ^{103}Pd . Furthermore, some of the photons that scatter from the rear hemisphere back into the front hemisphere must pass through the nominally 2.4 mm thick carrier a second time, resulting in an additional attenuation factor of about $e^{-1.01 * 0.24} / e^{-0.46 * 0.24} = 0.874$ for ^{125}I compared with water, and $e^{-1.96 * 0.24} / e^{-0.75 * 0.24} = 0.749$ for ^{103}Pd compared with water. This works out to a roughly 1% scatter deficit between the hemispheres.

Compared with homogeneous water, the Silastic carrier alone can be expected to reduce absorbed dose in the front

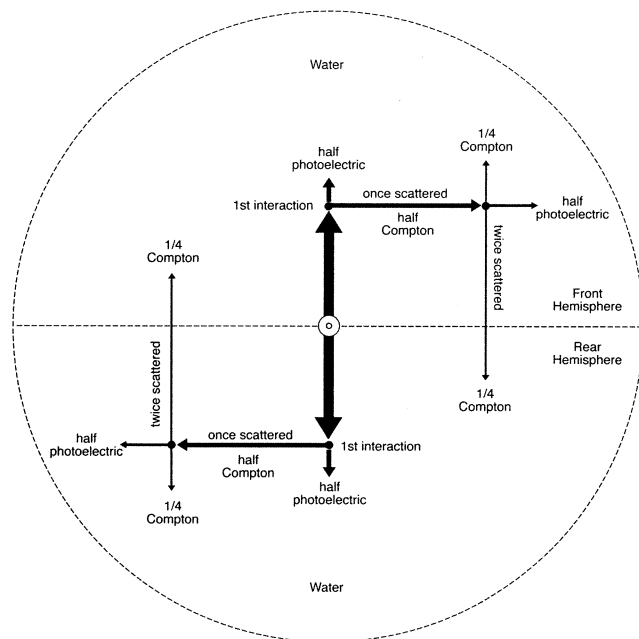


Fig. 6. A greatly simplified two-dimensional conceptual model of ^{125}I interactions with homogeneous water. The radial dose function $g(r)$ of the TG43 brachytherapy formalism assumes that a source is immersed in infinite homogeneous water. This figure also illustrates the full scatter geometry.

hemisphere by about 9% owing to primary attenuation in the carrier and by about another 1% owing to reduced scatter from the rear hemisphere. If air is present in the front hemisphere, the dose could be reduced by several percent more near the air interface. Chiu-Tsao *et al.* (4) calculated and measured about a 10% dose reduction at 1 cm for the carrier alone.

In Fig. 9 our point source is now inserted in a complete COMS plaque including both the gold backing and the Silastic carrier. In this case, we might speculate that the total dose reduction at any distance could be calculated as the product of the ratios plotted in Fig. 3 for the gold shell alone and the Silastic alone. The reason this does not work is that the gold fluorescence X-rays must now pass through the Silastic carrier before they can contribute to the water dose. At 13 keV about 94% of interactions in Silastic will be photoelectric, with a MFP of less than 1 mm. Very few of the gold fluorescence X-rays will escape the Silastic carrier, so the data for gold alone are no longer valid. The data for the Silastic alone are also invalid as they included backscatter, which is no longer present.

Compared with homogeneous water, the combination of gold plaque and Silastic carrier should reduce the absorbed dose in the front hemisphere by about 9% owing to photoelectric attenuation of primary radiation in the carrier, and by another 11% owing to lack of backscatter from the rear hemisphere. If air is present in the front hemisphere, the dose could be reduced by several percent more near the air interface. Looking at the data for Silastic plus gold (solid triangles) in infinite water in Fig. 3, we see a noisy, but

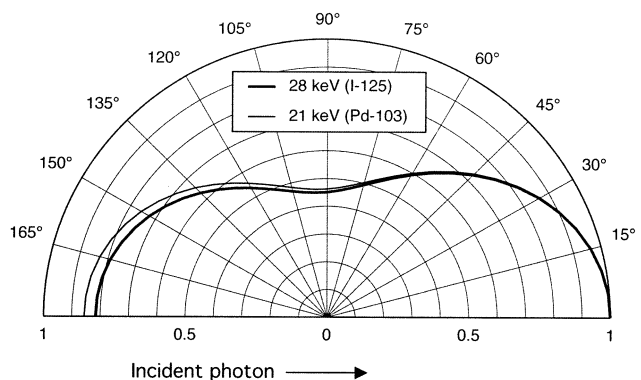


Fig. 5. Angular distribution of the differential Compton scattered photons per unit solid angle for 21 and 28 keV normalized to 1.0 at $\varphi = 0$ degrees. At these low energies the angular probability of scattering is roughly symmetric around $\varphi = 90$ degrees.

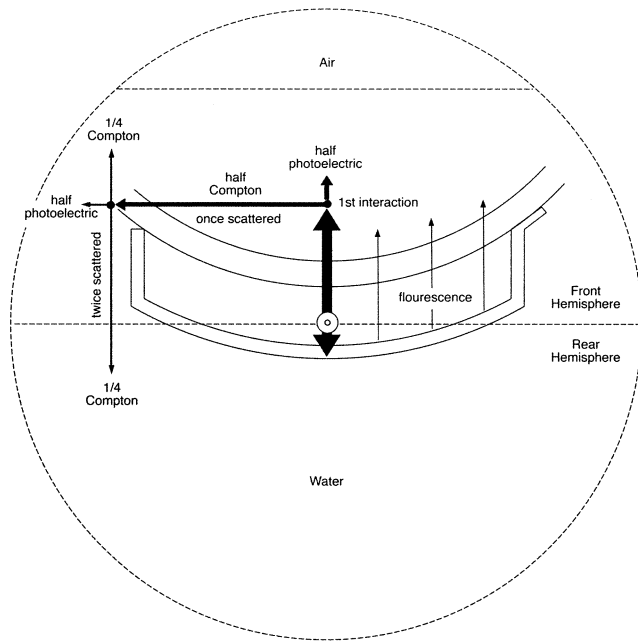


Fig. 7. A greatly simplified conceptual model of ¹²⁵I interactions in the presence of the gold backing alone, immersed in water, with an air-interface somewhere in front of the plaque. The gold backing eliminates backscatter that would otherwise have originated from behind the plaque but also adds fluorescent X-rays. Compared with homogeneous water, the net result is a small dose enhancement just in front of the plaque and a dose reduction at greater distances. This model also applies to plaques that do not use a Silastic carrier, such as those described by Luxton *et al.* (15, 22), Astrahan *et al.* (24), and Nag *et al.* (29).

decreasing ratio that appears to bottom out at approximately 0.8, about 16 mm from the source, yielding the anticipated 20% dose reduction. Considering the simplicity of the model presented in this conceptual discourse, it is remarkable how well it predicts the published measurements and far more sophisticated Monte Carlo calculations.

METHODS

The instantaneous dose rate from any individual seed at a point (r,φ) can be expressed according to the TG43 formalism (9) as:

$$D(r, \varphi)_{TG43} = S_k * \Lambda * g(r) * [G(r, \varphi)/G(r_0, \varphi_0)] * F(r, \varphi) \quad (2)$$

where r = distance between point p and the seed center, φ = the angle from the seed axis, S_k = air kerma strength of source in U (1 U = 1 cGy cm² h⁻¹), Λ = dose rate constant at 1 cm in cGy h⁻¹U⁻¹, g(r) = the radial dose function, G(r,φ) = the geometry factor, and F(r,φ) = the anisotropy function.

An existing TG43-based ophthalmic plaque planning system (Plaque Simulator [PS], BEBIG GmbH, Berlin, Germany) was modified to better account for interactions with the Silastic insert and eye-air interface. This software has been described previously (22–27). Over the past decade this software has been steadily revised to improve the planning of eye plaque therapy by addressing both the dosimetric calculation and the surgical procedure. Briefly, the PS software uses a combination of computed tomography (CT), magnetic

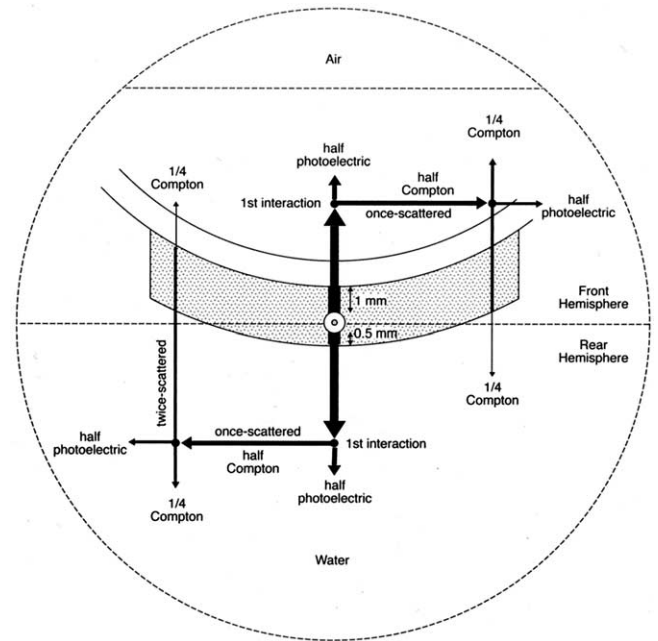


Fig. 8. A greatly simplified conceptual model of ¹²⁵I interactions in the presence of the COMS (Collaborative Ocular Melanoma Study) Silastic carrier alone, immersed in water, with an air-interface somewhere in front of the plaque. A Silastic carrier absorbs more radiation than would a water equivalent carrier, resulting in a relative dose reduction in all directions.

resonance imaging (MRI), ultrasonography, and fundus imaging to build a photorealistic 3D virtual model of the patient eye, as illustrated in Fig. 10. The posterior portion of the eye is modeled as a hemisphere, the anterior portion is modeled as an oblate spheroid that intersects the cornea. The dimensions and intersections of these geometric objects and the location of the optic nerve and lens are determined from CT or MRI images. Estimates of the location of muscle attachment are calculated. This allows the model to adapt to the specific eccentricities of each individual eye.

The PS software includes 3D models of all standard and notched COMS plaques that can be interactively loaded with seeds and positioned on the virtual eye. The Silastic carrier can be rotated in the gold shell. The 3D plaque models include details such as the suture eyelets for which coordinates on the eye surface can be calculated. These coordinates along with other preplanning information derived from the software are used to rehearse and accelerate the surgical procedure with a corresponding reduction in OR time and trauma to the patient. Full 3D as well as 2D dosimetry on planar and even spherical surfaces such as the retina are provided. Critical points-of-interest in the eye are located automatically and point dose calculations provided. Some of these features are illustrated in Fig. 11. The PS software also provides a backward compatible D_{COMS} calculation mode in addition to its more advanced features.

Before this work, the PS software applied a simple scalar correction factor T to the calculated dose of COMS plaques at all points to account for differences in scatter and attenuation between the Silastic-plus-gold combination and water, as:

$$D(r, \varphi, T) = D(r, \varphi)_{TG43} * T \quad (3)$$

The correction factor T = 0.9 was derived from the measure-

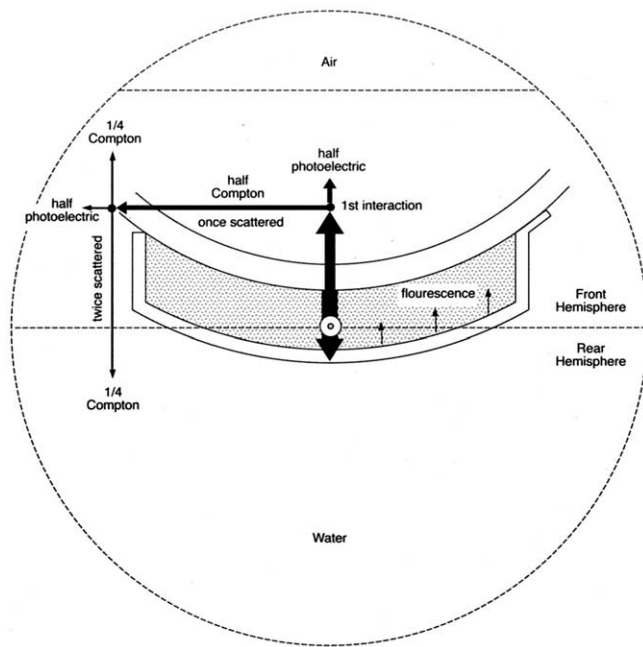


Fig. 9. A greatly simplified conceptual model of ^{125}I interactions in the presence of both the gold backing and Silastic carrier, immersed in water with an air-interface somewhere in front of the plaque. The gold backing eliminates backscatter that would otherwise have originated from behind the plaque. The Silastic carrier absorbs more radiation than would a water equivalent carrier, including all the fluorescent X-rays generated by the gold. The result is a significant dose reduction in front of the plaque compared with homogeneous water.

ments of Chiu-Tsao *et al.* (4) who reported an approximate 10% reduction at 1 cm on the central axis of the COMS 20 mm plaque. The factor **T** is specific to COMS plaques because it is a combined correction for both the gold and Silastic. The PS uses a different gold-only scatter and fluorescence correction based on the work of Luxton *et al.* (15) for plaques that do not use a Silastic carrier.

The factor **T** was revised for this work to account for the distance *r* between the seed center and the dose calculation point as illustrated in Fig. 12. The revised correction function **T**(*r*) is the curve illustrated in Fig. 3 that is a fifth order polynomial fit to the Silastic-plus-gold central axis Monte Carlo calculations of Chiu-Tsao *et al.* (4) assuming that the ratio to water bottoms out at 0.8. The function **T**(*r*) is also assumed to account for all scatter deficits caused by the gold plaque, but to account only for primary attenuation in a 1 mm thick spherical shell of Silastic surrounding the seed center. For points away from the source transverse axis, an additional path length in Silastic **d** is calculated, as also shown in Fig. 12. The ratio of attenuation in Silastic to attenuation in water for this additional path length **d** is estimated to be:

$$t(d, u) = e^{-\mu^*d} / e^{-\mu(\text{water})^*d} \quad (4)$$

The revised PS software was also used to calculate and plot the MLPS to points in the eye for fully loaded COMS 12 and 20 mm plaques. The seeds were modeled using the typical diameter of 0.8 mm and offset of 1 mm from the carrier surface, resulting in a distance of 1.4 mm between the seed axis and the carrier's concave surface. The MLPS was estimated as the sum of the direct linear path lengths (**d** + 1 mm in Fig. 12) in Silastic between the

calculation point and each seed's center divided by the number of seeds.

A new function **A**(*R*) was also introduced that implements the air-interface factor proposed by Zerda *et al.* (5):

$$A(R) = 0.85 + (0.1 * R) \quad R \leq 1.5 \text{ cm} \quad (5)$$

where *R* is the distance from the air interface. The eye-air interface is approximated as a plane perpendicular to the AP axis of the eye that crosses the cornea and is tangent to the minor apex of the oblate spheroid that defines the anterior portion of the eye. This plane is illustrated by the dashed line in Fig. 11.

The dose rate at any point *P* is calculated using the basic TG43 formalism $D(r, \varphi)_{\text{TG43}}$, and then modified by the factors **T**(*r*), **t**(*d*, μ), and **A**(*R*):

$$D(r, \varphi, d, \mu) = D(r, \varphi)_{\text{TG43}} * T(r) * t(d, \mu) * A(R) \quad (6)$$

RESULTS

Plotted in Fig. 13 are isoMLPS calculated on a plane bisecting fully loaded COMS 12 and 20 mm plaques. The MLPS is minimal near the center of the eye with an approximate magnitude of 1 mm. The minimum possible path length through Silastic is 1 mm because the seeds are oriented tangent to, but offset 1 mm from, the front surface of the carrier. The MLPS increases with off-axis distance and as one approaches the surface of the plaque. Immediately in front of the plaque the gradient is steep, ranging from an MLPS of approximately 3.8 mm at the external scleral surface to about 2.2 mm at the retina for the 20 mm plaque. The gradient in front of the 12 mm plaque is even steeper. Adjacent to the plaque, the MLPS to retina ranges from approximately 1.5–2 mm. The shaded region in front of the plaque represents a hypothetical tumor. Although the MLPS is quite inhomogeneous throughout much of the tumor region, for most tumors the MLPS will be at its smallest in the vicinity of the apex. The actual value will depend on the tumor's height and shape and also on the diameter of the plaque. For medium to tall tumors, the MLPS at the tumor apex will probably fall somewhere in the range 1–1.3 mm.

The revised PS software was used to calculate dose distributions for a single model 6711 seed centered in a COMS 20 mm plaque immersed in pure water, mimicking the Monte Carlo calculations of Chiu-Tsao *et al.* (4). The PS dose rate constant Λ was modified to 0.85 [the currently recommended value of Λ for model 6711 ^{125}I seeds is 0.98 (28)] to match that used in their calculations. In Fig. 14, the PS isodose lines are superimposed on a rescaled copy of Fig. 7 from Chiu-Tsao *et al.* (4). The only readily apparent difference between the two calculations occurs outside the eye near the source axis. That is may be due to PS's simplification of the TG43 anisotropy function **F**(*r*, φ) to **F**(φ) for fixed *r* = 10 mm.

Plotted in Fig. 15 is a PS calculation mimicking the conditions of the TLD measurements of Zerda *et al.* (5), a

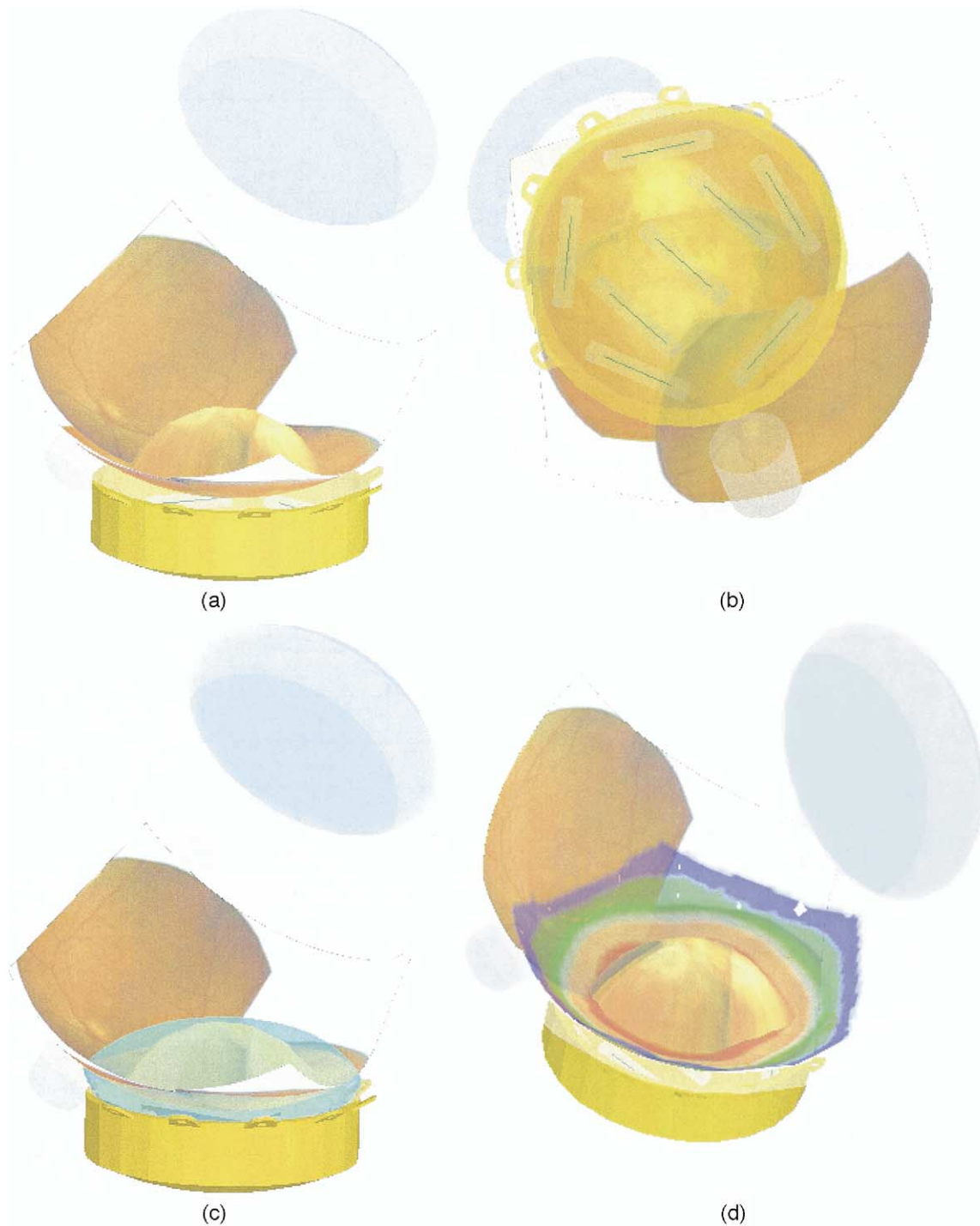


Fig. 10. The Plaque Simulator software builds a fully interactive, photorealistic three-dimensional model of each patient's eye and tumor from a composite of computed tomography, magnetic resonance, ultrasonography, and fundus imaging. (a) The dimensions of the eye are determined from computed tomography or magnetic resonance imaging, the tumor from ultrasonography. Fundus photographs are then mapped back onto the retinal and tumor surfaces. (b) The software's ability to render any or all surfaces translucently helps when choosing which plaque to use for a particular tumor, which seed slots to load, and how to best orient the suture eyelets. (c) Isodose surfaces can be displayed in full three dimensions, or (d) as dose distributions on surfaces such as the retina.

single ^{125}I seed centered in a COMS 20 mm plaque in their eye-head phantom. This calculation includes air-interface correction. The PS isodose lines are superimposed on a rescaled copy of Fig. 6b from Zerda *et al.* (5). The PS dose

rate constant Λ was modified to be 0.88 to match the pre-NIST99 ^{125}I calibrations in effect at the time of their measurements.

Figure 16A, B, and C compares isodose plots for a 20 mm

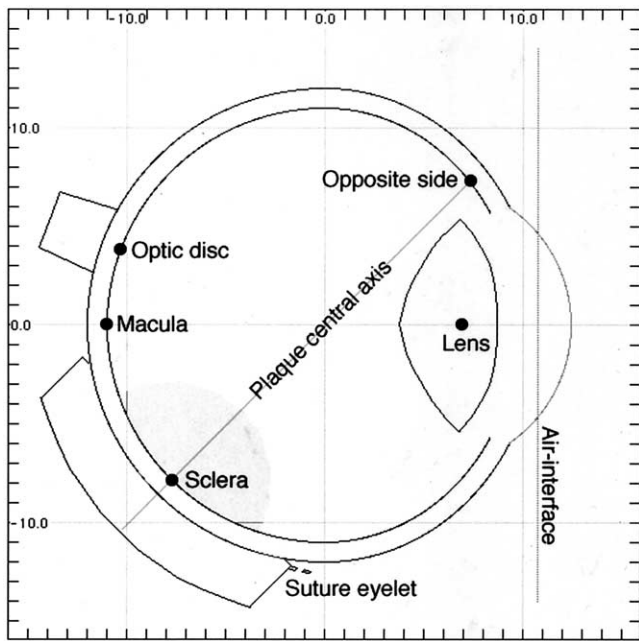


Fig. 11. Illustrated here are the locations of the points-of-interest for which dose rates are calculated in Tables 4 and 5. The location of the eye-air-interface plane is also illustrated.

plaque fully loaded with 24 1 mCi seeds for (A) the COMS dosimetry model D_{COMS} , (B) the earlier PS model $D(r, \varphi, T)$, and (C) the current PS model $D(r, \varphi, d, \mu)$. This arrangement is typical of what might be employed to treat a large, equatorially located tumor. Note that the isodose curves are slightly asymmetric with respect to the plaque central axis due to the air interface at the cornea. The corresponding dose rates at some ocular structures that would be reported under the COMS protocol are listed in Table 4. The scleral dose rate is calculated at a point 1 mm inset from the external surface of the eye on the central axis of the plaque. The macular dose rate is calculated 1 mm inset from the external surface of the eye at the posterior pole. The lens dose rate is calculated at the center of the lens coordinate system. These points are illustrated in Fig. 11. For this particular plaque and location, the $D(r, \varphi, d, \mu)$ calculations are 20%–27% less than would be reported under the D_{COMS}

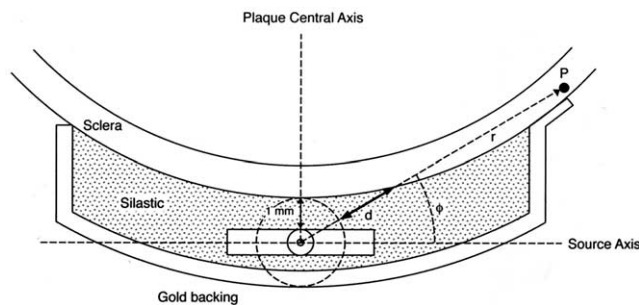
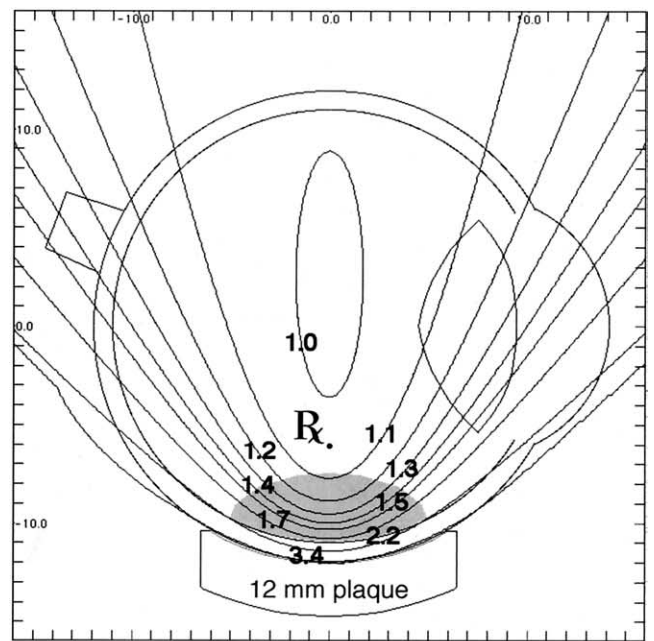
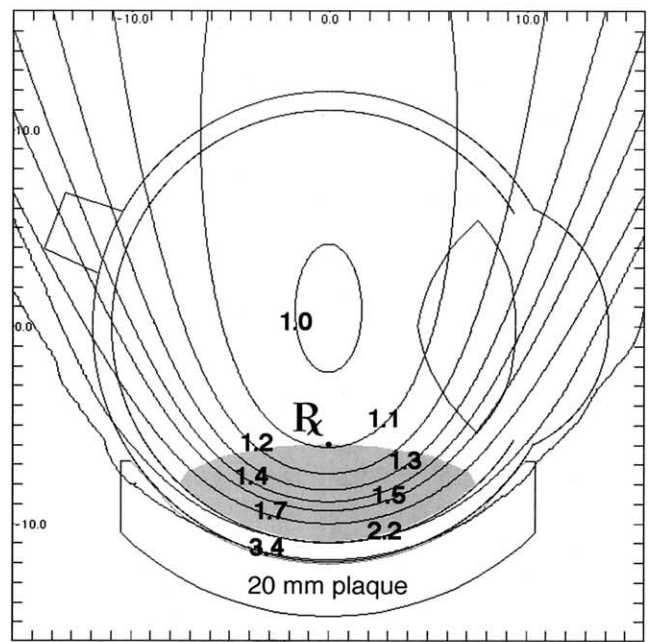


Fig. 12. The geometry used to calculate the factors $T(r)$ and $t(d, \mu)$ that account for central axis and off-axis attenuation in the Silastic carrier. The distance d is the extra thickness of Silastic that off-axis primary radiation must pass through to reach point P.



(a)



(b)

Fig. 13. Plotted here are isopath lengths (mm) representing the mean linear path through Silastic (MLPS) between each calculation point and all seed centers for (a) a COMS (Collaborative Ocular Melanoma Study) 12 mm plaque fully loaded with 8 ^{125}I seeds, and (b) a COMS 20 mm plaque fully loaded with 24 seeds. The MLPS is minimal (approximately 1 mm) near the center of the eye and increases with distance off-axis and with proximity to the carrier surface. The shaded region in front of the plaque represents a hypothetical tumor. The tumor apex is a good candidate for the dose prescription point because the MLPS to the apex is generally close to its minimum value of 1 mm, thereby minimizing dosimetric uncertainty (compared with homogeneous water) associated with the Silastic. Conversely, dosimetric uncertainty associated with the Silastic will be greatest immediately in front of and adjacent to the plaque where the magnitude and gradient of the MLPS are both large.

protocol. Compared with the previous PS calculation $D(r,\varphi,T)$, the dose to structures in the posterior hemisphere is about 13% lower, whereas the lens is about 20% lower. Dose to sclera in front of the plaque is 6% lower.

Figure 17A, B, and C compares isodose plots for a 12 mm COMS plaque fully loaded with 8 1 mCi seeds for (A) the COMS dosimetry model D_{COMS} , (B) the earlier PS model $D(r,\varphi,T)$, and (C) the current PS model $D(r,\varphi,d,\mu)$. This arrangement is typical of what might be used to treat a small, posteriorly located tumor. The corresponding dose rates at the same ocular structures as before are listed in Table 5. For this particular plaque and location, the $D(r,\varphi,d,\mu)$ calculations are 16%–50% less than would be reported under the D_{COMS} protocol. Compared with the previous PS calculation $D(r,\varphi,T)$, the dose to structures adjacent to the plaque in the posterior hemisphere is about 13% lower, whereas anterior locations are about 20% lower. Dose to sclera in front of the plaque is only 1% less. Dose rate on the plaque central axis for the three cases depicted in Fig. 17 is plotted in Fig. 18.

DISCUSSION

Chiu-Tsao *et al.* (4) confirmed that fluorescent X-rays originating from the gold backing are absorbed in the Silastic seed carrier by demonstrating the absence of dose enhancement in front of the plaque, but their conclusion that “the effect of the Silastic insert alone was found to be closely the same as the Silastic/gold combination” was unexpected. The dominant effect of the Silastic carrier alone should be to isotropically remove more photons through photoelectric absorption than would have been absorbed if the carrier volume were water equivalent. Secondary effects would be that proportionally less Compton scatter originates from the carrier volume, and some scatter that originates from behind the plaque will be more rapidly attenuated as it recrosses the Silastic carrier compared with a water equivalent carrier. At 1 cm in front of the plaque, these effects can

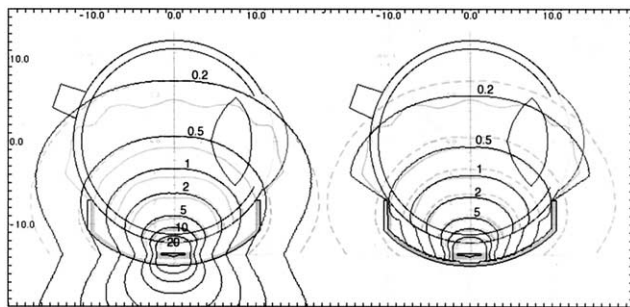


Fig. 14. Plaque simulator isodose calculations (black lines) for a single ^{125}I seed in (a) infinite homogeneous water and (b) centered in a 20 mm COMS (Collaborative Ocular Melanoma Study) plaque immersed in infinite water are superimposed on copies of the equivalent Monte Carlo calculations (pale gray lines) of Fig. 7 from Chiu-Tsao *et al.* (4). The broken lines in the Chiu-Tsao figures are the isodose lines in homogeneous water. Dose rates are in cGy/h for a 1 mCi source.

be summarized as a primary attenuation factor $F_{\text{Si-primary}}$ with a magnitude of about 10%, and a backscatter deficit factor $F_{\text{Si-scatter}}$ with a magnitude of roughly 1%.

One effect of the gold backing is to contribute fluorescence X-rays to the radiation emitted toward the front of the plaque. Without the Silastic carrier, that would result in a localized dose enhancement $F_{\text{Au-fluorescence}}$ with a magnitude of a few percent in the space (water) that would ordinarily be occupied by the carrier and for a few mm beyond. When the carrier is made of Silastic, nearly all fluorescence from the gold is photoelectrically absorbed in the carrier itself, so no dose enhancement is seen in the water.

Another important effect of the gold backing is to prevent primary radiation from entering a roughly hemispherical volume behind the plaque, thereby preventing scatter from originating out of that volume. The material from which the carrier is made should have little effect on the gold's absorption of rearward directed radiation. A scatter deficit

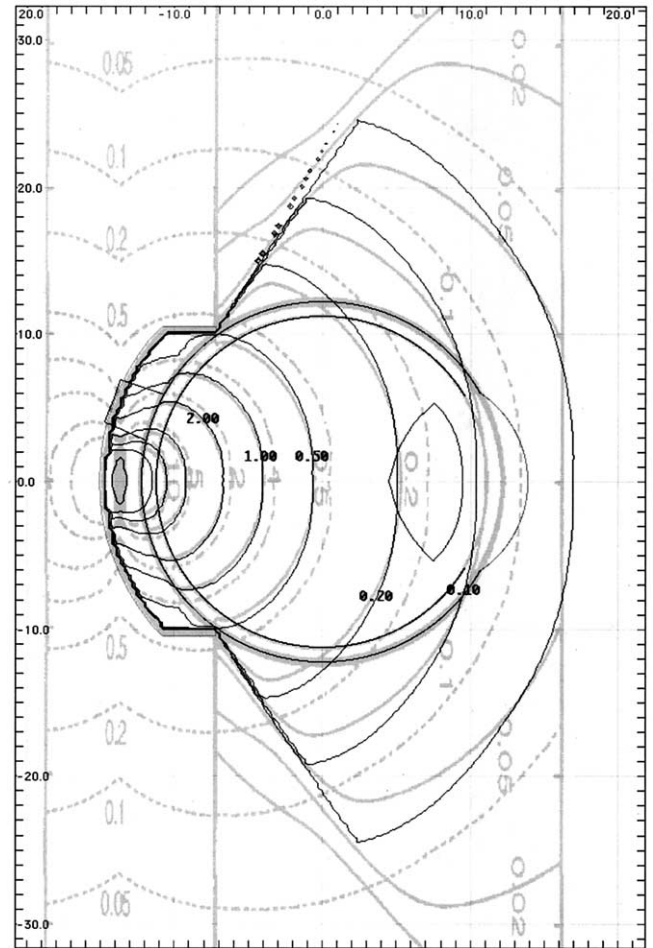


Fig. 15. Plaque simulator isodose calculations (black lines) for a single ^{125}I seed in centered in a 20 mm COMS (Collaborative Ocular Melanoma Study) plaque immersed in water with a nearby air interface are superimposed on a copy of the calculations (pale gray lines) from Fig. 6b of Zerda *et al.* (5) for the equivalent situation. The broken lines in the Zerda plot are isodose lines in homogeneous water, the solid lines are for the plaque in eye-head phantom. Dose rates are in cGy/h for a 1 mCi source.

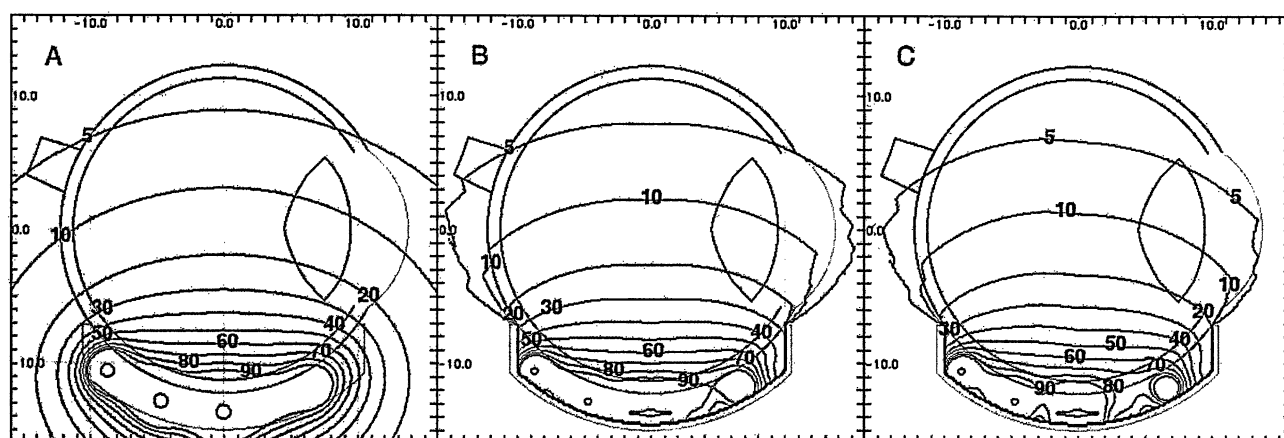


Fig. 16. Twenty-four 1 mCi ^{125}I seeds were installed in a COMS (Collaborative Ocular Melanoma Study) 20 mm plaque located on equator of 12.3 mm radius eye. Point dose rate measurements at the locations illustrated in Fig. 11 are listed in Table 4. Dose rates in cGy/h were calculated using (A) the required D_{COMS} protocol, (B) the original Plaque Simulator method $D(r,\varphi,T)$, and (C) the enhanced Plaque Simulator methodology $D(r,\varphi,d,\mu)$.

$F_{\text{Au-scatter}}$ of magnitude about 10% at 1 cm in front of the plaque, attributable to the near-complete lack of backscatter from the rear hemisphere, should still occur. The dose at 1 cm in the presence of the Silastic carrier alone should be reduced by the factors $F_{\text{Si-primary}}$ and $F_{\text{Si-scatter}}$, and in the presence of the Silastic-plus-gold combination by the factors $F_{\text{Si-primary}}$, $F_{\text{Si-scatter}}$, and $F_{\text{Au-scatter}}$. Thus, the ratio of dose to water should be noticeably lower in the case of the Silastic-plus-gold combination than for Silastic alone. Chiu-Tsao *et al.* (4) state that statistical tests were performed to compare the two sets of ratios, but it was “inconclusive whether the results were significantly different” for the two configurations. In examining their data as redrawn here in Fig. 3, it appears that most of the Silastic-plus-gold points (black triangles) do fall below both the Silastic-alone points (white squares) and gold-alone points (white circles). The problem is that the data are noisy. For example, in the range 9–11 mm, the ratios for Silastic-plus-gold range between 0.81 and 0.91. By visual inspection, the value of 0.91 at 10.4 mm appears to be an outlier. With only 8 points for Silastic alone, it is difficult to identify a consistent trend in the results. With 18 points, it was possible to fit a curve to the Silastic-plus-gold data as illustrated in Fig. 3 and use this as the basis for the $T(r)$ factor introduced above.

Many of the dosimetric issues addressed herein were

recognized at the time the COMS was designed. In fact, chapter 12 of the COMS Manual of Procedures (10) states: “The effect of the gold plaque and the Silastic insert on dose to the target volume is to be neglected until the magnitude of these effects can be unequivocally determined in the physics literature.” Unfortunately, brachytherapy dosimetry software capable of dealing with these issues was not widely available at the time the study was begun. In addition, there were significant uncertainties in the calibration and dosimetry of ^{125}I , the TG43 report would not be published for another decade, and computers with the speed, memory, and displays required to make 3D treatment planning and Monte Carlo modeling practical were not yet widely affordable. Monte Carlo methods have the advantage, in principle, of being able to elegantly deal with both plaque and tissue inhomogeneities and can produce excellent results when compared with measurement, but they are time consuming to develop and compute, and their complexity makes that approach difficult to incorporate and support in a practical treatment planning system at this time. The article by Krintz *et al.* (6) appears to indicate that we have now reached the point at which the physics literature is sufficient to begin accounting for these factors. The approach described in this work is a practical application of

Table 4. Calculated dose rates at various points of interest for 24 1 mCi seeds in a COMS 20 mm plaque located at the equator of a 12.3 mm radius eye, as illustrated in Fig. 15

Location	D_{COMS} cGy/h	$D(r,\varphi,T)$ cGy/h	$D(r,\varphi,d,\mu)$ cGy/h	$D(r,\varphi,d,\mu)/$ $D(r,\varphi,T)$	$D(r,\varphi,d,\mu)/$ D_{COMS}
Optic disk	6.569	6.048	5.278	0.87	0.80
Macula	9.985	8.993	7.796	0.87	0.78
Lens	12.55	11.58	9.268	0.80	0.74
Opposite retina	4.095	3.454	2.981	0.86	0.73
Sclera	110.2	94.26	88.23	0.94	0.80

Abbreviation: COMS = Collaborative Ocular Melanoma Study.

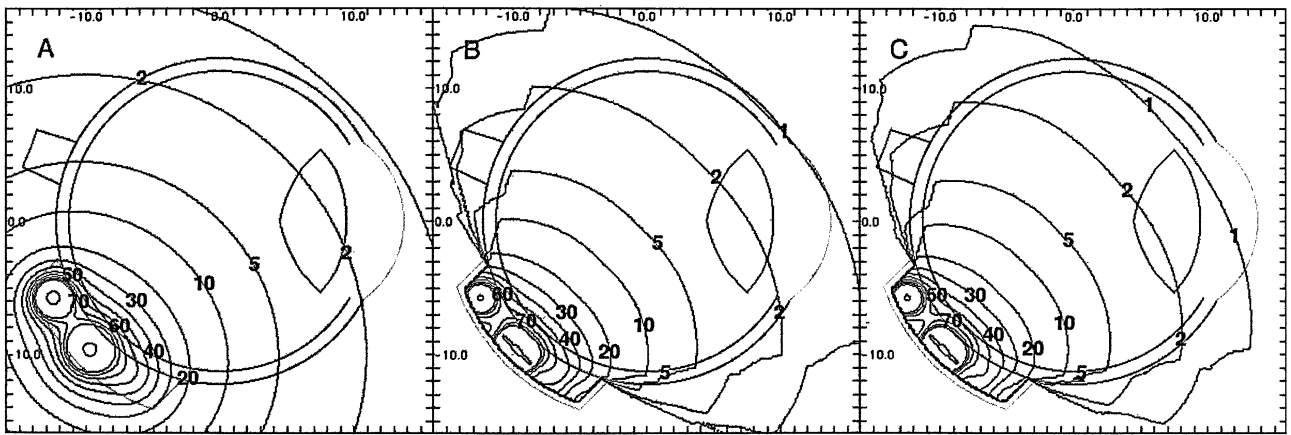


Fig. 17. Eight 1 mCi ^{125}I seeds were installed in a COMS (Collaborative Ocular Melanoma Study) 12 mm plaque located midway between the posterior pole and equator of a 12.3 mm radius eye. Point dose rate measurements at the locations illustrated in Fig. 11 are listed in Table 5. Dose rates in cGy/h were calculated using (A) the required D_{COMS} protocol, (B) the original Plaque Simulator method $D(r, \varphi, T)$, and (C) the enhanced Plaque Simulator methodology $D(r, \varphi, d, \mu)$.

the available data and has shown good agreement with measurements and more complex models.

From Fig. 13 we see that if the Silastic is not accounted for during dose calculation, prescribing dose at heights of 3 mm or less could result in significant dosimetric uncertainty (compared with homogeneous water) due to the large magnitude and steep gradient of the MLPS near the plaque. According to the COMS protocol, dose is to be prescribed at the apex of the tumor (e.g., Fig. 13b) for tumors 5 mm or greater in apical height, and at 5 mm from the interior surface of the sclera (e.g., Fig. 13a) for tumors from 2.5–5 mm in apical height. As shown in Fig. 13, these prescription points are good choices because they are locations at which the MLPS is close to its minimum value of 1 mm, and these points are also beyond the range of any gold fluorescence effects.

Most choroidal melanomas occur in the posterior hemisphere. As illustrated in Fig. 18, dose on the central axis of a plaque being used to treat a posterior tumor is only weakly influenced by the PS change from the $D(r, \varphi, T)$ calculation to the new $D(r, \varphi, d, \mu)$ model. This result is consistent with Fig. 13, where we observe that the MLPS ranges from 1 to about 1.3 mm for points on or near the plaque axis at distances greater than about 3 mm (depending on the plaque size) from the plaque surface. On the other hand, dose to

retina adjacent to the plaque, where the MLPS varies from approximately 1.5–2 mm, decreased by about 13%. Some of the difference is due to the new $T(r)$ factor, some to the $t(d, \mu)$ off-axis factor. The air-interface factor $A(R)$ becomes insignificant around the equator and therefore does not affect dosimetry in the posterior part of the eye. The effect of $A(R)$ will become noticeable primarily when studying dose to the cornea, lens, or ciliary bodies. In some studies, dose to the inner surface of the eye opposite the plaque is followed. For extremely posterior tumors, the opposite side of the eye will be close to the limbus and thus close to air. The calculated dose to a point on the opposite side of the eye from a posteriorly located plaque will be noticeably lower when the air-interface factor is included. For anterior tumors, the plaque will also be located anteriorly, and there will be some overlap between the $T(r)$ and $A(R)$ factors because each is attempting to correct for reduced scatter from what are now overlapping volumes. Until this issue can be resolved, the air-interface correction should not be used when planning anterior tumors.

Finger *et al.* (8) have recently proposed a prospective randomized clinical trial comparing ^{106}Ru , ^{125}I , and ^{103}Pd . The lower E_{avg} of ^{103}Pd compared with ^{125}I is attractive in terms of reducing dose to the eye opposite the plaque. However, ^{103}Pd will also deliver a higher dose to the tumor

Table 5. Calculated dose rates at various points of interest for eight 1 mCi seeds in a COMS 12 mm plaque located midway between the posterior pole and equator of a 12.3 mm radius eye as illustrated in Fig. 16

Location	D_{COMS} cGy/h	$D(r, \varphi, T)$ cGy/h	$D(r, \varphi, d, \mu)$ cGy/h	$D(r, \varphi, d, \mu)/$ $D(r, \varphi, T)$	$D(r, \varphi, d, \mu)/$ D_{COMS}
Optic disk	5.327	3.561	3.072	0.86	0.58
Macula	11.75	6.747	5.851	0.87	0.50
Lens	2.184	2.010	1.599	0.80	0.73
Opposite side	1.279	1.077	0.855	0.79	0.67
Sclera	69.34	58.58	58.00	0.99	0.84

Abbreviation as in Table 4.

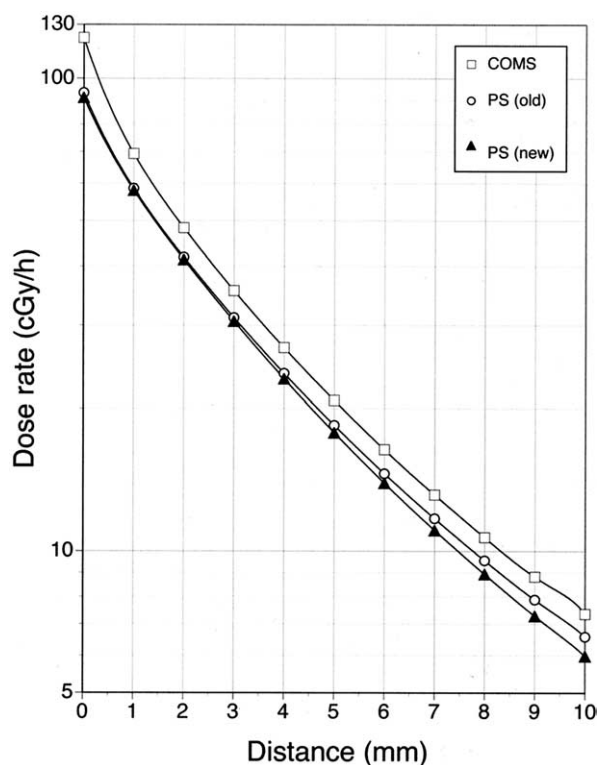


Fig. 18. Dose rate on the plaque central axis for the three cases shown in Fig. 17. Distance is from the inner surface of the carrier that is touching the external sclera of the eye. The white squares are the D_{COMS} protocol, the white circles the old Plaque Simulator method $D(r, \varphi, T)$, and the black triangles the new Plaque Simulator methodology $D(r, \varphi, d, \mu)$.

base and possibly to locations adjacent to the plaque than will ^{125}I for the same height tumor. Being primarily a beta emitter, ^{106}Ru has its own unique dosimetric issues (27). To provide the same accuracy of treatment planning for ^{103}Pd as is now possible for ^{125}I , studies for ^{103}Pd similar to those of Zerda *et al.* (5) will be required to correct for extraocular air; and studies similar to those of Chiu-Tsao *et al.* (4) will

be required if the ^{103}Pd seeds are to be used in an eye plaque that employs a Silastic carrier, or, for that matter, a carrier of any material (e.g., an acrylic such as Lucite) whose effective atomic number differs significantly from that of water. Until such data become available, ^{103}Pd should not be used in plaques with Silastic carriers. Plaques such as those described by Luxton *et al.* (15, 22), Astrahan *et al.* (25), and Nag *et al.* (29) do not use a carrier at all, making them better suited for ^{103}Pd use. The seeds are glued directly to or into shallow grooves or collimating slots in the concave surface of the gold backing using a thin film of cyanoacrylate adhesive. By placing the seeds in very close proximity to a collimating surface, geometric penumbra is minimized, and much of the laterally directed radiation that does not contribute to the tumor dose can be eliminated (25), thereby sparing critical structures (e.g., macula or optic nerve) adjacent to the plaque. Astrahan's (25) slotted design also isolates the seeds from one another with gold septa so there can be no interaction with the silver or titanium of an adjacent seed. These plaques still require a correction factor for the effects of the gold plaque alone (15) and for the air-interface.

CONCLUSION

In their reanalysis of the COMS medium tumor trial data, Krintz *et al.* (6) concluded that "the amount of reduction in the dose to structures of interest could be clinically significant, so future eye plaque dosimetry should be performed using the most up-to-date parameters available." Dose calculations for ^{125}I seeds in COMS eye plaques that accurately account for the linear source geometry, anisotropy, collimation by the plaque backing and lip, geometric penumbra, scatter reduction due to the gold backing and extraocular air, and attenuation (both on-axis and off-axis) in the Silastic carrier are both possible and practical, and have been implemented in the software described in this work.

REFERENCES

1. Collaborative Ocular Melanoma Study Group. The COMS randomized trial of iodine 125 brachytherapy for choroidal melanoma. III. Initial mortality findings. COMS report no. 18. *Arch Ophthalmol* 2001;119: 969–982.
2. Kline RW, Yeakel PD. Ocular melanoma, I-125 plaques [Abstract]. *Med Phys* 1987;14:475.
3. Astrahan M, Luxton G, Jozsef G, Kampp TD, Liggett P, Sapozink MD. An interactive treatment planning system for ophthalmic plaque radiotherapy. *Int J Radiat Oncol Biol Phys* 1990;18:679–687.
4. Chiu-Tsao S-T, Anderson LL, O'Brien K, Stabile L, Liu JC. Dosimetry for 125I seed (model 6711) in eye plaques. *Med Phys* 1993;20:383–389.
5. Zerda A, Chiu-Tsao S-T, Lin J, *et al.* ^{125}I seed eye plaque dose distribution including penumbra characteristics. *Med Phys* 1996;23:407–418.
6. Krintz AL, Hanson WF, Ibbott GS, Followill DS. A reanalysis of the Collaborative Ocular Melanoma Study medium tumor trial eye plaque dosimetry. *Int J Radiat Oncol Biol Phys* 2003;56:889–898.
7. Finger PT, Lu DF, Buffa A, De Blasio DS, Bosworth JL. Palladium-103 versus iodine-125 for ophthalmic plaque radiotherapy. *Int J Radiat Oncol Biol Phys* 1993;27:849–854.
8. Finger PT, Berson A, Tracy N, Szechter A. Palladium-103 plaque radiotherapy for choroidal melanoma: An 11 year study. *Int J Radiat Oncol Biol Phys* 2002;54:1438–1445.
9. Nath R, Anderson LL, Luxton G, Weaver KA, Williamson JF, Meigooni AS. Dosimetry of interstitial brachytherapy sources: Recommendations of the AAPM radiation therapy committee task group no. 43. *Med Phys* 1995;24:209–234.
10. Collaborative Ocular Melanoma Study Group. COMS manual of procedures, Ch 12—radiation therapy, version 2/99, PB95–179693. Springfield, VA: National Technical Information Service; 1995.
11. Hubbell JH, Seltzer SM. Tables of X-ray mass attenuation coefficients and mass energy-absorption coefficients (version

- 1.03). Available at: <http://physics.nist.gov/PhysRefData/XrayMassCoef/cover.html>. Gaithersburg, MD: National Institute of Standards and Technology; 1997. (Originally published as NISTIR 5632, National Institute of Standards and Technology, Gaithersburg, MD; 1995.) Accessed in December 2003.
12. Mayneord WV. The significance of the röntgen. *Acta Int Union Against Cancer* 1937;2:271.
 13. Khan FM. The physics of radiation therapy. 3rd ed. Philadelphia: Lippincott Williams & Wilkins; 2003.
 14. Weaver KA. The dosimetry of ^{125}I seed eye plaques. *Med Phys* 1986;13:78–83.
 15. Luxton G, Astrahan MA, Petrovich Z. Backscatter measurements from a single seed of ^{125}I for ophthalmic plaque dosimetry. *Med Phys* 1988;15:397–400.
 16. Wu A, Sternick ES, Muise DJ. Effect of gold shielding on the dosimetry of an ^{125}I seed at close range. *Med Phys* 1988;15:627–628.
 17. Cygler J, Szanto J, Soubra M, Rogers DWO. Effects of gold and silver backings on the dose rate around an ^{125}I seed. *Med Phys* 1990;17:172–178.
 18. Wu A, Krasin F. Film dosimetry analyses on the effect of gold shielding for iodine-125 eye plaque therapy for choroidal melanoma. *Med Phys* 1990;17:843–846.
 19. Meli JA, Motakabbir KA. The effect of lead, gold and silver backings on dose near ^{125}I seeds. *Med Phys* 1993;20:1251–1256.
 20. Flühs D, Heintz M, Indenkampen F, Wiczorek C, Kolanoski H, Quast U. Direct reading measurement of absorbed dose with plastic scintillators. The general concept and applications to ophthalmic plaque dosimetry. *Med Phys* 1996;23:427–434.
 21. Dale RG. Some theoretical derivations relating to the tissue dosimetry of brachytherapy nuclides, with particular reference to iodine-125. *Med Phys* 1983;10:176–183.
 22. Luxton G, Astrahan MA, Liggett P, Neblett DL, Cohen DM, Petrovich Z. Dosimetric calculations and measurements of gold plaque ophthalmic irradiators using iridium-192 and iodine-125 seeds. *Int J Radiat Oncol Biol Phys*, 1988;15:167–176.
 23. Astrahan M, Luxton G, Jozsef G, Liggett P, Petrovich Z. Optimization of I-125 ophthalmic plaque brachytherapy. *Med Phys* 1990;17:1053–1057.
 24. Evans MDC, Astrahan MA, Bate R. Tumor localization using fundus view photography for episcleral plaque therapy. *Med Phys* 1993;20:769–775.
 25. Astrahan MA, Luxton G, Pu Q, Petrovich Z. Conformal episcleral plaque therapy. *Int J Radiat Oncol Biol Phys* 1997;39:505–519.
 26. Knutsen S, Hafslund R, Monge OR, *et al.* Dosimetric verification of a dedicated 3D treatment planning system for episcleral plaque therapy. *Int J Radiat Oncol Biol Phys* 2001;51:1159–1166.
 27. Astrahan MA. A patch source model for treatment planning of ruthenium ophthalmic applicators. *Med Phys* 2003;30:1219–1228.
 28. Williamson JF, Coursey BM, DeWerd LA, Hanson WF, Nath R, Ibbott G. Guidance to users of Nycomed Amersham and North American Scientific Inc. I-125 interstitial sources: Dosimetry and calibration changes, recommendations of the American Association of Physicists in Medicine radiation therapy committee ad hoc subcommittee on low-energy seed dosimetry. *Med Phys* 1999;26:570–572.
 29. Nag S, Wang D, Wu H, Bauer CJ, Chambers RB, Davidorf FH. Custom-made “Nag” eye plaques for ^{125}I brachytherapy. *Int J Radiat Oncol Biol Phys* 2003;56:1373–1380.